Low-temperature Schottky barrier tunneling in InSb/$In_xAl_{1-x}Sb$ quantum well heterostructures

A. M. Gilbertson,[1,2] J. M. S. Orr,[1,3] P. D. Buckle,[1] S. Clowes,[2] M. Fearn,[1] C. J. Storey,[1] L. Buckle,[1] L. F. Cohen,[2] and T. Ashley[1]

[1]*QinetiQ, St. Andrews Road, Malvern, Worcestershire WR14 3PS, United Kingdom*

[2]*Blackett Laboratory, Imperial College London, Prince Consort Road, London SW7 2BZ, United Kingdom*

[3]*School of Electrical and Electronic Engineering, University of Manchester, Sackville Street, Manchester M60 1QD, United Kingdom*

(Received 21 March 2007; published 6 August 2007)

We report low-temperature $I(V)$ measurements taken on small area surface metal contacts to InSb/InAlSb quantum well material in the temperature range 4.5–100 K. We obtain Schottky barrier $J(V)$ data under reverse bias and analyze the transport observed by using a tunneling model derived from the three-dimensional density of states, showing close correlation for the majority of devices measured. We consider the "Rowell" analysis [*Tunneling Phenomena in Solids*, edited by E. Burnstein and S. Lundqvist (Plenum, New York, 1969), p. 273] of the zero-bias resistance $R_0(T)$ and differential conductance $G(V)$ for determining the dominant transport mechanism. Two distinct temperature dependences are observed in the $R_0(T)$ data, a weak insulatorlike dependence identifying true single-step tunneling and a strong nonlinear dependence, which we attribute to defect assisted multistep tunneling. Effective barrier parameters are extracted by fitting the $G(V)$ data with a Brinkman-Dynes-Rowell model [J. Appl. Phys. **41**, 5 (1970)] for carrier tunneling.

DOI: 10.1103/PhysRevB.76.085306 PACS number(s): 73.43.Jn, 73.61.Ey, 73.20.−r

INTRODUCTION

The injection of spin-polarized electrons from ferromagnetic metals into nonmagnetic semiconductors remains a topic of great interest for semiconductor spintronics due largely to the scarcity of usable room temperature magnetic semiconductors [$T_{\mathrm{Curie}} <$ room temperature (RT)].[1] Significant progress has been made in recent years in understanding the physics of ferromagnetic metal-semiconductor contacts and the mechanisms that govern spin injection. It has been shown that it is virtually impossible to inject sizable spin-polarized current from a ferromagnetic metal into a semiconductor through a simple Ohmic contact due to the large conductivity mismatch of the differing materials at the interface.[2] Significant spin polarization can be restored by the introduction of a large spin-preserving interface resistance, $r_b^*(\Omega\ \mathrm{m}^2)$, such as a tunnel barrier in the form of an ultrathin dielectric (such as a metal oxide) or an engineered Schottky barrier.[1,2] It has been shown theoretically that significant magnetoresistance can only be observed over a narrow range of r_b^* values, dependent on material parameters and device geometry.[1] For efficient spin injection, the barrier resistance is not restricted by an upper limit and must only exceed a threshold value related to the resistivity and spin diffusion length of the semiconductor; moreover, there is no requirement for symmetric characteristics on forward and reverse bias (as only forward bias is important). For spin transistor type structures where both injection and detection of spin are necessary,[3] the requirements on both the barrier properties and characteristics are far less trivial to satisfy.[1,4]

Schottky barriers formed at most metal/*n*-type semiconductor interfaces provide a natural tunnel barrier to electrons without the difficulty of producing a discrete, pinhole-free dielectric/oxide layer. The shape and width of the Schottky barrier is predominantly determined by the space charge present in the depletion layer as a result of the inclusion of extrinsic doping. It has been shown that the depletion region resulting from Schottky barrier formation is detrimental to spin injection,[5] unless the shape and width is engineered to minimize these effects such as deleterious carrier accumulation and scattering (see Refs. 4 and 5). Recent advances in GaAs/AlGaAs heterostructures have demonstrated successful spin injection from a magnetic metal into a semiconductor using both CoFe/MgO metal-oxide and Fe/AlGaAs engineered Schottky tunnel barriers, achieving 52% (at 100 K) and 32% (at 4.5 K) spin polarizations, respectively.[6,7]

For spintronic applications, narrow band-gap semiconductors, such as InAs and InSb, may offer advantages over their wider gap counterparts, such as GaAs and Si, due to their high electron mobility and large spin-orbit coupling, offering greater potential for spin manipulation via the intrinsic Rashba field induced from the structural inversion asymmetry inherent in quantum well (QW) heterostructures.[8] InSb has the lightest electron effective mass and largest g factor (~ -51) of all the III-V semiconductors, along with a strong spin-orbit coupling. Recent advances in InSb/InAlSb QW field effect transistors[9] (FETs) make this system attractive for developing hybrid spintronic technology. Recent studies on spin lifetime in InSb epitaxial layers, as well as in wide InSb QW structures,[10] suggest that InSb could be more attractive over InAs based devices for spintronic applications.[11] Room temperature Schottky barrier transport in InSb/InAlSb QW FETs has been reported, where results show good agreement with standard thermionic emission (TE) theory, confirming the presence of a Schottky barrier.[12]

In this paper, we present low-temperature Schottky barrier $I(V)$ data from measurements on InAlSb/InSb QW material. Detailed understanding of the barrier design and subsequent transport characteristics will be essential for developing useful spin injection and/or detection devices. Experimental results are compared with modeled data to complement previous work on these structures,[12] and as a prerequisite for future efforts to engineer the Schottky barrier for efficient spin injection according to the criteria of Fert and Jaffres.[1]

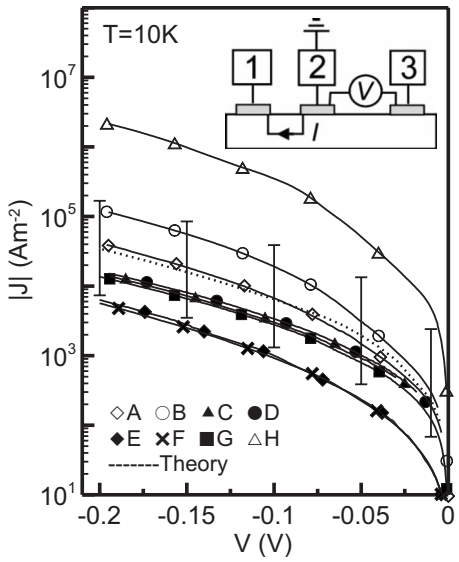

FIG. 1. Reverse bias $J(V)$ characteristics at 10 K for a number of InSb/InAlSb QW Schottky barrier devices labeled A–H and the corresponding fit (dashed line) from band profile modeling of the structure using Eq. (1). Inset shows a schematic diagram of the three terminal measurement setup.

Samples were grown by solid source molecular-beam epitaxy onto a semi-insulating GaAs (001) substrate. In growth order, the heterostructure consists of an accommodation layer, a 3 μm $In_{0.85}Al_{0.15}Sb$ buffer layer, a 15 nm InSb QW, and a 50 nm $In_{0.8}Al_{0.2}Sb$ cap with Te modulation-doping layer located 5 nm above the QW. This forms a type-I heterostructure, providing two-dimensional (2D) confinement for both electrons and holes in the QW channel. Hall measurements on this material determined the mobility to be 62 000 (26 500) cm^2 V^{-1} s^{-1} at 77 K (RT) and the carrier concentration to be 9.3×10^{11} (1.0×10^{12}) cm^2 at 77 K (RT). Devices were processed using optical lithography to define source and drain Ohmic contacts and e-beam lithography to define small area Schottky contacts. Schottky contacts are formed by Ti/Au bilayers deposited by e-beam evaporation, and are typically 200 nm in length. A wet chemical etch is used to electrically isolate devices and form the active transport mesas, with widths ranging from 3 to 12 μm. Air bridges are formed from the Schottky contact to the feed metal as a result of the mesa isolation to allow small area contacting with the intention of minimizing leakage.

RESULTS AND DISCUSSION

Samples were measured in a liquid helium bath cryostat over a range of temperatures from 4.5 to 100 K. A three terminal measurement was performed to obtain the barrier characteristics. The measurement setup is shown in the inset of Fig. 1. Current is passed between contact 1 (Ohmic) and contact 2 (Schottky), and an adjacent remote contact 3 (also Ohmic) is used to measure the voltage dropped with respect to earth. Providing no current is passed between the earthed Schottky contact (2), and the remote contact (3), the $I(V)$ characteristic of the Schottky barrier beneath contact 2 can be measured independently from the channel conductivity and contact resistance of the Ohmic contacts 1 and 3. Reverse bias $J(V)$ characteristics of eight typical devices are presented in Fig. 1 by using the nominal area estimated from scanning electron microscopy images of the Schottky contacts. The data exhibit a large variation in magnitude, although grouping into clusters is observed. This clustering is discussed later.

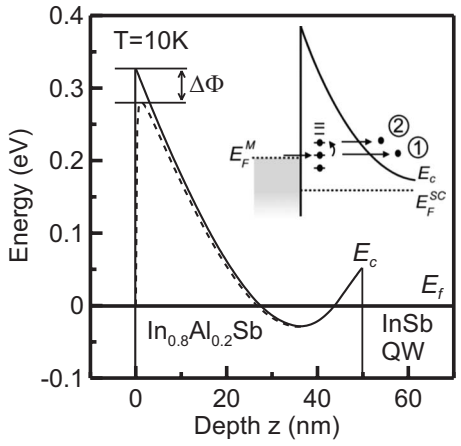

FIG. 2. Schrödinger-Poisson solution of a heavily doped InSb/InAlSb heterostructure at 10 K (solid lines), in the region of the Schottky tunnel barrier at zero applied bias. The effect of image charge at the metal-semiconductor interface is shown by the dashed line. Inset shows a schematic diagram of a multistep tunneling mechanism (Ref. 13).

It is expected at these low temperatures that the contribution from TE is minimal, and consequently, reverse bias $J(V)$ will be dominated by tunneling through the Schottky barrier. Tunneling current is dependent on the transmission coefficient $T(E)$ of the Schottky barrier and the Fermi-Dirac occupation distributions $F(E)$ in the metal and the semiconductor. A band profile for the heavily doped $In_{0.8}Al_{0.2}Sb$ Schottky tunnel barrier under investigation is presented in Fig. 2. This is calculated from a self-consistent Schrödinger-Poisson model (SPM) tailored to narrow band-gap materials and is used to obtain band profiles and transmission coefficients of the active injection region.[13] The material parameters used in these calculations were derived from transmission spectroscopy performed by Dai *et al.* to determine the band-gap energy of $In_{1-x}Al_xSb$.[14] The band gaps of the $In_{0.8}Al_{0.2}Sb$ barrier layers and the unstrained (strained) InSb QW at 100 K are taken to be 640 and 230 meV (261 meV), respectively.[14] The conduction:valence band offset is taken to be 62%:38% following Ref. 15. It is assumed in this analysis that the Fermi energy is pinned at midgap on the semiconductor surface, following measurements undertaken in similar material systems.[12,15] In the model, midgap pinning at the surface was ensured by forcing a potential at the surface (left hand) boundary of the Schrödinger-Poisson calculation (Fig. 2).

To calculate the tunneling current density J_T, we start with the relation $J=nqv$, which can be expressed as $dJ(E) \equiv qv[N(E)/V]dE$, where n is the volume density of carriers taken from the three-dimensional (3D) density of states $N(E)$

(valid in the barrier region where the electron is tunneling), q the electron charge, and v the characteristic electron velocity.[16] The tunneling current density J_T for injection into the semiconductor (under reverse bias) is then proportional to $J(E)$ multiplied by the transmission coefficient $T(E)$, the occupation probability in the metal $F_M(E)$, and the probability of unoccupied states in the semiconductor $[1-F_{SC}(E)]$. The resulting overall expression for $J_T=J(E)T(E)F_M(E)[1-F_{SC}(E)]$ is shown in Eq. (1) in expanded form,

$$J_T = A^* \frac{\sqrt{2m^*}}{4(\pi k_b)^3} v \int_0^{\phi_b} E^{1/2} T(E) F_M(E)[1 - F_{SC}(E)]dE, \quad (1)$$

where A^* is the effective Richardson constant,[16] m^* is the effective mass in the barrier, and k_b is the Boltzmann constant. $J(V)$ characteristics are simulated by evaluating the integral in Eq. (1) numerically for a range of reverse bias conditions, using data obtained from SPM calculations. Data points generated from this model are indicated by the dashed line in Fig. 1 and show good agreement with the measured $J(V)$ characteristics. Error bars plotted are derived from a nominal ±10% uncertainty in the total top barrier thickness of the structure. Due to the exponential dependence of $T(E)$ on the barrier thickness, error bars span an order of magnitude encompassing the majority of low current data sets. All devices show good functional fit to this model.

Although a good fit of the modeled tunnel current density suggests electron transport via tunneling, this alone is insufficient to conclude that it is the dominant or sole transport mechanism. To determine further the nature of the transport, we have considered the criteria set out by Rowell *et al.*[17] to identify single-step elastic electron tunneling in superconductor-insulator-superconductor (*S-I-S*) structures. Only three of the criteria set out by Rowell apply when neither electrode is superconducting: (a) an exponential conductance dependence on barrier thickness, (b) parabolic behavior of the conductance-voltage $[G(V)]$ that can be fitted to standard barrier models, and (c) a weak insulatorlike temperature dependence of the zero-bias resistance $R_0(T)$. In magnetic tunnel junction (MTJ) literature, the second criterion is most commonly used; however, a recent study by Akerman *et al.*[18] revealed that only the third criterion can be used as a definitive test for an integral tunnel barrier, since successful fits can be made to $G(V)$ data by the Simmons[19] and Brinkman-Dynes-Rowell (BDR)[20] tunneling models even when subsequently shown to include pinholes.[18] Figure 3 shows $R_0(T)$ data for a number of devices studied. In this case, the zero-bias resistance is taken from a linear interpolation fit about $V=0$. Two very distinct temperature dependences are observed from the data: a weak insulatinglike linear temperature dependence for devices C and D, satisfying the third Rowell criterion (inset of Fig. 3) and a much stronger temperature dependence for devices A, B, and H. It can be assumed directly from this analysis that devices C and D demonstrate single-step tunneling through an integral tunnel barrier. The regular alternative $R_0(T)$ dependence, commonly attributed to a pinholed barrier, is a metalliclike behavior, where the $R_0(T)$ exhibits the opposite temperature dependence, i.e., a linear dependence with positive gradient;[18] however, this is also very different from the temperature dependence observed for these higher conductance devices.

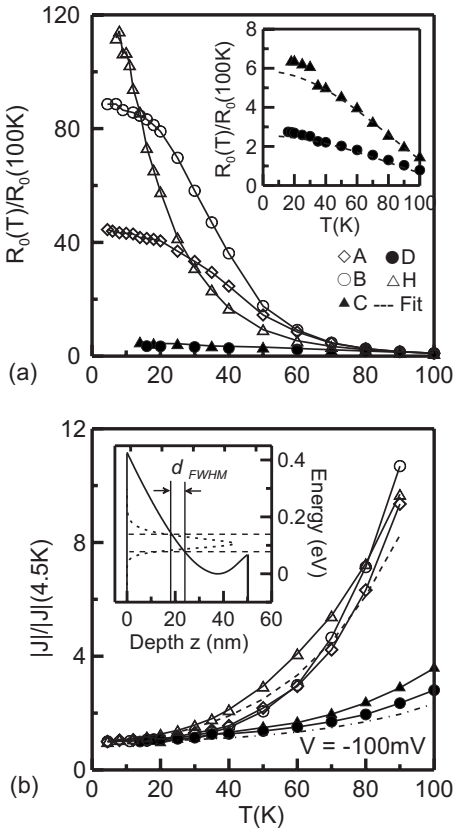

FIG. 3. (a) Normalized zero-bias resistance as a function of temperature for five Ti/InAlSb Schottky tunnel barriers studied up to 100 K exhibiting single-step and multistep tunneling. Inset shows devices C and D plotted on a reduced resistance scale to show the linear dependence more clearly (dashed lines indicate fit to Stratton tunneling model). (b) Normalized absolute gate current density at −100 mV as a function of temperature. Dashed line indicates fit from simple defect assisted tunneling model; dashed-dot line shows the fit from Eq. (1) for direct tunneling. Inset shows the Schrödinger-Poisson solution of the band profile at −100 mV (solid line) and corresponding tunneling probability (dashed line) estimating a barrier width d_{FWHM}.

In examining these $R_0(T)$ data, we consider the effect of defect assisted transport. Atomic force microscopy studies reveal typical threading dislocation densities of around 10^8 cm^{-2}. For the small area contacts considered in this study, assuming a uniform spatial distribution of defects, this corresponds to the order of single dislocations being present under the Schottky contact region (statistically one to three dislocations, dependent on mesa size and, therefore, gate area). The clustering observed in the data in Fig. 1 may, therefore, indicate enhanced or parallel transport as a result of a discrete number of defects within the barrier material, as a result of the presence of threading dislocations. A similar qualitative model has been proposed by Carrano *et al.* as a transport mechanism in GaN metal-semiconductor Schottky contacts[21] and a more recent quantitative model by Karmalkar *et al.*,[22] where electrons are allowed to tunnel into

deep level interface states associated with the presence of defects created by threading dislocations or the Ti adhesion layer incorporated in the metallization process. This so-called hopping, discussed previously in detail by Xu *et al.*,[23] is illustrated as a schematic diagram in the inset of Fig. 2. By this mechanism, electrons can tunnel into available states within the barrier, and then tunnel across the remaining barrier (process 1 of Fig. 2 inset) or be thermally excited up a ladderlike distribution of states within the barrier to then traverse the remaining (reduced) barrier at a higher energy (process 2 of Fig. 2 inset). Multistep tunneling via localized defect states is thought to be an incoherent, spin-flip scattering process[24] due to the mixing of tunneling electron wave functions with the nonpolarized defect states in the barrier.[25] Such an incoherent process would, thus, be detrimental to spin polarization. Tunneling magnetoresistance (TMR) studies in ferromagnetic tunnel junctions have confirmed this by showing that the inclusion of nonmagnetic impurities in the barrier (providing allowed states for the sequential hopping across the barrier) gives rise to extra conductance that is unpolarized, significantly reducing the TMR.[25] It is, however, worth noting that at higher temperatures ($T>200$ K), transport in InSb QW transistors is not dominated by tunneling or, indeed, trap assisted tunneling through the barrier, but is then controlled by the process of thermionic emission over the barrier, as reported earlier.[12] As a result, the presence of traps or detects in the barrier region will have no influence on the conductance of the barrier and hence device characteristics at elevated temperatures.[9]

$R_0(T)$ data from devices A and B show an unusual switch between the two temperature dependences at ~25 K, suggesting a breakdown in single-step tunneling [Fig. 3(a)]. The corresponding characteristic thermal activation or ionization energy attributed to the defect state ($\sim kT$) is of the order of 2 meV, suggesting defect states situated very close to the Fermi energy. This switching is not observed in all devices demonstrating strong $R_0(T)$ dependence and, indeed, not in the highest conduction device (H), suggesting that defect states in this device are fixed on or extend below the Fermi energy. This is consistent with the large influence on the $J(V)$ characteristics resulting from the mechanism being on resonance at zero bias.

In addition to the Rowel analysis of $R_0(T)$ data, we have analyzed the temperature dependence of the current density $J(T)$ to further clarify the influence of defect states in the barrier on tunneling current. In this analysis, a finite bias (−100 mV) of suitable magnitude is chosen to remove any ambiguity from low bias noise. Figure 3(b) shows the current density as a function of temperature, normalized by $J(4.5\ \mathrm{K})$, for the same five samples A, B, C, D, and H discussed above. Two distinct temperature dependences are again observed: a weak temperature dependence for devices C and D that demonstrate true single-step tunneling, which can be simulated using Eq. (1) [dashed-dotted line in Fig. 3(b)], and an increased temperature dependence for devices A, B, and H where contributions from mechanisms other than direct tunneling are thought to be present.

The increased temperature dependence observed in the $J(T)$ data qualitatively supports the idea of a distribution of enhanced transmission states in the barrier. With increasing temperature, carriers can be thermally excited either in the injection region or in the localized states, before traversing the barrier. For discrete states in energy up the barrier, this opens enhanced conductance channels *in parallel* with the direct tunneling conductance. We have simulated this by adding into the transport model enhanced transmission at discrete energies up the barrier. This is indicated in Fig. 3(b) by the dashed line and shows good agreement with the observed temperature dependence when the enhanced transmission states have a Gaussian tail-like distribution from the Fermi energy rather than a uniform distribution. States situated sufficiently below the Fermi energy would contribute only to the magnitude of J and not to the temperature dependence.

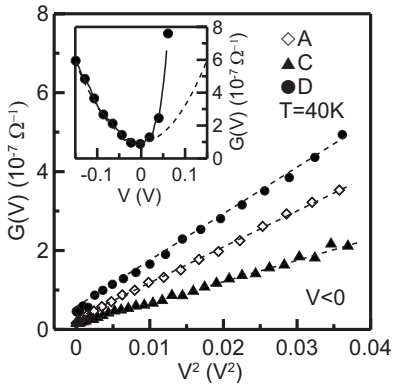

FIG. 4. Differential conductance as a function of voltage squared $G(V^2)$ at 40 K for devices A, C, and D in the negative bias regime. Inset shows the differential conductance for device D showing large asymmetry. Fits to the BDR model are indicated by dashed lines.

Parameters for the barrier region were extracted by fitting the Stratton tunneling model[26,27] to $R_0(T)$ data for $T>35$ K for devices C and D (deviation from Stratton behavior is observed in device C for $T<35$ K due to the onset of an anomalous drop in barrier conductance). The dashed lines in the inset of Fig. 3(a) indicate fits of this model to experimental data, from which we obtain barrier widths $d=47$ nm and barrier heights $\varphi_b=233$ meV for device C, and $d=46.5$ nm and $\varphi_b=229$ meV for device D.

In addition to the Stratton model, the BDR tunneling model was used to fit the differential conductance $G(V)$ and extract estimates for barrier parameters d and φ_b (also supporting transport via a single-step tunneling process according to the second Rowel criterion).[20] The analysis of $G(V)$ data is insightful when considering not only spin injection but also potential spin detection, since barrier properties such as bias asymmetry become important. The BDR model accounts for asymmetric barriers by including as adjustable parameters the barrier heights at the two classical boundaries φ_1 (metal-insulator) and φ_2 (insulator-semiconductor) and also the average barrier height φ_b. In our analysis, a triangular barrier is assumed by setting $\varphi_2=0$ meV in the calculations. Figure 4 shows the differential conductance as a function of the square of the gate voltage at 40 K [$G(V^2)$] for devices A, C, and D in the negative bias region. It can be seen that devices C and D, which demonstrate single-step

tunneling, follow a parabolic behavior up to −200 mV. Device A, proposed to support multistep tunneling, also shows parabolic behavior up to −200 mV. This is consistent with the conjecture of defect assisted tunneling and also supports the findings of Akerman *et al.*,[18] whereby successful fits of the BDR model were made to barrier $G(V)$, where single-step tunneling was determined not to be the dominant transport mechanism. The appearance of a zero-bias anomaly in the conductance is often observed at low temperatures in MTJ literature, and is commonly described as an attribute of tunneling. This strong feature in the $G(V)$ (Ref. 27) is often detrimental to the fitting of the BDR model as the region of parabolic behavior in the data is reduced. It is worth noting that in the structures measured here, no zero-bias anomaly is observed over the temperature range under examination; as a result, allowing more convincing fits of the BDR model to $G(V)|_{V<0}$ to be made. The dashed lines in Fig. 4 indicate fits of the BDR model to the data, from which we obtain $d=18$ nm and $\varphi_b=295$ meV for C, and $d=17.5$ nm and $\varphi_b=275$ meV for D. The higher conductance of device D compared to C is consistent with the presence of a narrower and lower barrier; however, the explanation for the observed conductance of device A, positioned between C and D, is less obvious. Extracted barrier parameters for device A yielded a significantly larger barrier width of $d=40$ nm compared to those of C and D and, therefore, we speculate that the competition between the enhanced conductance via hopping and the reduced conductance by the wide barrier results in the magnitude of the observed conductance. $G(V)$ data for all devices exhibit a large asymmetry due to the rectifying nature of the Schottky barrier, as demonstrated for device D in the inset of Fig. 4. Parabolic dependence in the positive bias regime was also observed up to +50 mV in all devices at 40 K (not shown here). This value decreases with increasing temperature as carriers have increased energy to surmount the barrier, thus reducing the effective barrier height and the bias at which TE begins to compete with tunneling.

A large discrepancy in the extracted barrier parameters is found between the two tunnel models, with the Stratton model yielding lower and wider barriers. The effective Schottky barrier varies with temperature due to the temperature dependence of the band gap and the onset of thermionic and thermionic-field emissions. This temperature dependence of barrier parameters consequently makes the Stratton model (which fits over a range of temperatures) less suitable in determining Schottky barrier parameters. Barrier parameters extracted from the BDR model at a finite low temperature are, therefore, taken here to be more reliable, although it is important to note that the importance of the BDR model fit lies not with the extracted values of d and φ_b, but more with the observation of parabolic behavior.[20] The Schottky barrier under reverse bias (−100 mV) is shown in the inset of Fig. 3(b). Indicated by the dashed line, the functions within the integral of Eq. (1) combine to give an effective tunneling "flux" such that the probability of carriers tunneling through the barrier is distributed over energy (strongly influenced by temperature) about a peak centered on the Fermi energy. Taking the full width at half maximum (FWHM) of this distribution as the energy range over which the majority of carriers will tunnel, it can be seen that the width of the barrier d can be estimated to lie over a range varying between ~17 and 24 nm. Therefore, the smaller estimated barrier widths from the BDR model are not unreasonable for an approximately triangular barrier, exhibiting a narrower average width based on band profile modeling and Eq. (1). In addition to the above, we have also considered the effect of image force lowering of the Schottky barrier (dashed line Fig. 2), whereby the barrier height is lowered by an amount given by the expression[16]

$$\Delta\varphi_b = \left(\frac{q\xi_{\max}}{4\pi\varepsilon_S}\right)^{1/2}, \tag{2}$$

where $\xi_{\max}$ is the maximum field at the metal-semiconductor interface, and ε_s is the semiconductor permittivity (taken to be $16.45\varepsilon_o$ for $In_{0.8}Al_{0.2}Sb$ from Ref. 14). From the examination of the conduction band gradient at the interface, taken from calculated SPM calculations, where $\xi_{\max}=-dV/dx|_{x=0}$, it can be shown that the Schottky barrier is lowered by an amount $\Delta\varphi_b \approx 40$ meV for the range of biases considered. From the above considerations, the barrier parameters extracted from the BDR model are seen to show good agreement with expected parameters based on band profile modeling [Fig. 2 and inset of Fig. 3(b)] and, therefore, also the assertion that the InAlSb material system exhibits midgap pinning at the metal-semiconductor interface.[12]

Typical r_b^* values for barriers measured are of the order of $10^{-5}\ \Omega\ m^2$ at −50 mV. For the purpose of spin injection, this is ~6 orders of magnitude greater than the threshold value, which in the case of a two-dimensional electron gas is the product $\rho_N^{2D}W \sim 10^{-11}\ \Omega\ m^2$ (where ρ_N^{2D} is equal to the 2D sheet resistivity multiplied by the spin diffusion length, and W is the barrier contact length[28]) and, therefore, satisfying the condition for significant spin polarization to be restored at the interface. This r_b^* value is, however, too large to observe any sizable magnetoresistance according to theoretical predictions.[1,28] This is not surprising, however, as the material studied in this paper has a thick top barrier of 50 nm and has not been engineered to specifically reduce the Schottky barrier width. In the region where parabolic behavior is observed in the positive bias regime, r_b^* values for barriers measured are of the order of $10^{-6}\ \Omega\ m^2$ (+50 mV). For all electrical spin injection and detection, the tunnel barrier must have a suitable interface resistance but should also be symmetric with respect to bias. The results shown here do not fulfil these requirements, but do show that careful analysis is required to determine tunneling transport, and demonstrates the potential for the use of $In_{1-x}Al_xSb$ Schottky tunnel barriers for spin injection and detection by showing parabolic $G(V)$ behavior between −200 and +50 mV. Engineering of the extrinsic doping in the barrier region to reduce the depletion width and bias dependence will increase the symmetry in $G(V)$ and reduce the interface resistance significantly.

CONCLUSIONS

We have analyzed Schottky barrier tunneling in $InSb/In_{1-x}Al_xSb$ QW devices, using three tunneling models

to fit observed temperature dependence and conductance variation. Of the two standard barrier models considered, we have found the BDR model to generate the most reasonable parameters, as supported by band profile modeling. With the observation of single-step tunneling, we have demonstrated the ability to use an InAlSb Schottky barrier as a tunnel barrier suitable for spin injection. The differential conductance of most samples measured follows a parabolic dependence up to 200 mV in the negative bias regime and up to 50 mV in the positive regime.

We have demonstrated that the strong temperature dependence observed in $R_0(T)$ data is consistent with a multistep tunneling process via localized states in the Schottky barrier. We have demonstrated that analysis of $R_0(T)$ data can be used in this material system to determine the dominant transport mechanism and have also shown that the temperature dependence of the current at finite bias can be used as a means of identifying defect or trap assisted multistep tunneling from direct tunneling.

ACKNOWLEDGMENT

This work was supported by the UK EPSRC.

[1] A. Fert and H. Jaffres, Phys. Rev. B **64**, 184420 (2001).
[2] G. Schmidt and L. W. Molenkamp, Semicond. Sci. Technol. **17**, 310 (2002).
[3] S. Datta and B. Das, Appl. Phys. Lett. **56**, 665 (1990).
[4] W. Van Roy, P. Dorpe, J. De Boeck, and G. Borghs, Mater. Sci. Eng., B **126**, 155 (2006).
[5] J. D. Albrecht and D. L. Smith, Phys. Rev. B **68**, 035340 (2003).
[6] X. Jiang, R. Wang, R. M. Shelby, R. M. Macfarlane, S. R. Bank, J. S. Harris, and S. S. P. Parkin, Phys. Rev. Lett. **94**, 056601 (2005).
[7] A. T. Hanbicki, O. M. J. van't Evre, R. Magno, G. Kioseoglou, C. H. Li, and B. T. Jonker, Appl. Phys. Lett. **82**, 4092 (2003).
[8] M. E. Flatte, *Semiconductor Spintronics and Quantum Computation* (Springer, New York, 2002).
[9] S. Datta *et al.*, Tech. Dig. - Int. Electron Devices Meet. **2005**, 783 (2005).
[10] K. L. Litvinenko, L. Nikzad, J. Allam, B. N. Murdin, J. J. Harris, L. F. Cohen, and C. R. Pidgeon (unpublished).
[11] K. L. Litvinenko, L. Nikzad, J. Allam, B. N. Murdin, C. R. Pidgeon, J. J. Harris, T. Zhang, and L. F. Cohen J. Appl. Phys. **101**, 083105 (2007).
[12] J. M. S. Orr, P. D. Buckle, M. Fearn, P. J. Wilding, C. J. Bartlett, M. T. Emeny, L. Buckle, and T. Ashley, Semicond. Sci. Technol. **21**, 1408 (2006).
[13] I. H. Tan, G. L. Snider, L. D. Chang, and E. L. Hu, J. Appl. Phys. **68**, 4071 (1990).
[14] N. Dai, F. Brown, R. E. Doezema, S. J. Chung, K. J. Goldammer, and M. B. Santos, Appl. Phys. Lett. **73**, 21 (1998).
[15] N. Dai, G. A. Khodaparast, F. Brown, R. E. Doezema, S. J. Chung, and M. B. Santos, Appl. Phys. Lett. **76**, 26 (2000).
[16] E. H. Rhoderick, *Metal-Semiconductor Contacts* (Clarendon, Oxford, 1978).
[17] J. M. Rowell, in *Tunneling Phenomena in Solids*, edited by E. Burnstein and S. Lundqvist (Plenum, New York, 1969), p. 273.
[18] J. J. Akerman, R. Escudero, C. Leighton, S. Kim, D. A. Rabson, R. W. Dave, J. M. Slaughter, and I. K. Schuller, J. Magn. Magn. Mater. **240**, 86 (2002).
[19] T. E. Hartman, J. Appl. Phys. **35**, 11 (1964).
[20] W. F. Brinkman, R. C. Dynes, and J. M. Rowell, J. Appl. Phys. **41**, 5 (1915).
[21] J. C. Carrano, T. Li, P. A. Grudowski, C. J. Eiting, R. D. Dupuis, and J. C. Campbell, Appl. Phys. Lett. **72**, 542 (1998).
[22] S. Karmalkar, D. M. Sathaiya, and M. S. Shur, Appl. Phys. Lett. **82**, 22 (2003).
[23] Y. Xu, A. Matsuda, and M. R. Beasley, Phys. Rev. B **42**, 1492 (1990).
[24] J. M. Lawrence, Y. C. Chen, G. H. Kwei, M. F. Hundley, and J. D. Thompson, Phys. Rev. B **56**, 5 (1997).
[25] R. Jansen and J. S. Moodera, Phys. Rev. B **61**, 9047 (2000).
[26] Y. Li and S. X. Wang, J. Appl. Phys. **91**, 7950 (2002).
[27] B. Oliver and J. Nowak, J. Appl. Phys. **95**, 546 (2004).
[28] H. Jaffres and A. Fert, J. Appl. Phys. **91**, 10 (2002).